Research Square

Preprints are preliminary reports that have not undergone peer review.
They should not be considered conclusive, used to inform clinical practice,
or referenced by the media as validated information.

Reproducing Solar Spectral Irradiance by LEDs

Anton Kopatsch
Helmholtz Zentrum München
Peter Kary
Helmholtz Zentrum München
Mustafa Özden
Helmholtz Zentrum München
Andreas Albert
Helmholtz Zentrum München
Andrea Ghirardo
Helmholtz Zentrum München
Jana Winkler
Helmholtz Zentrum München
Gunther Seckmeyer
University of Hannover
Jörg-Peter Schnitzler (jp.schnitzler@helmholtz-muenchen.de)
Helmholtz Zentrum München

Research Article

Keywords: LEDs, ultraviolet, infrared

Posted Date: December 1st, 2020

DOI: https://doi.org/10.21203/rs.3.rs-112770/v1

License: This work is licensed under a Creative Commons Attribution 4.0 International License.
Read Full License

Abstract

The development of light-emitting diodes (LEDs) of different emission spectra is revolutionizing lighting technology and opening up completely new applications and research areas. The spectral irradiance of the sun reaching the Earth's surface is very complex due to radiative transfer processes within the atmosphere and ranges from the shortwave ultraviolet (UV) to longwave infrared (IR) radiation. The simulation of this spectral irradiance by artificial light sources is technically very demanding. It could be realized sufficiently so far by a combination of different light sources, mostly light bulbs, metal halide lamps and fluorescent tubes, in combination of different filters. In the present work, we are presenting a new LED Sun Simulator system, which allows simulating spectral irradiance close to natural solar spectral irradiance from 360 to 800 nm. The system generates the spectral irradiance by a combination of 23 different types of LED. The irradiance of each of the 23 different LED types can be separately controlled by software to modulate the spectra. In total, the system comprises 2,530 high-power LEDs mounted on 100 printed circuit boards (PCBs) / aluminum boards. With this system, an experimental area of one square meter can be homogeneously irradiated (irradiance with a mean variability of 2 % in the integrated range of 360 nm - 800 nm) at the distance of 1.6 m simulating the spectral irradiance of the standard reference spectrum of the American Society for Testing and Materials (ASTM G173-03). At maximum, the LED lighting field can reach an irradiance of 2,500 W m^{-2}, which is more than twice than that of the brightest sunlight in Central Europe. Thus, the new system opens up multiple new applications in many research areas ranging from photobiology to human health and environmental and material sciences.

Introduction

For billions of years, our sun has been, directly or indirectly, the most important source of energy for all biogeochemical and biological processes taking place on Earth. Most of the organisms living on Earth today, humans, animals, plants and microorganisms have adapted to the radiance of the sun during the course of evolution. However, the solar spectral irradiance reaching the Earth's surface is not identical to the extraterrestrial solar spectral irradiance above the Earth's atmosphere and changes dynamically throughout the Earth's history [1] with distinct annual and diurnal variations [2]. Atmospheric gases surrounding the Earth, such as water vapor, CO_2, ozone, lead to an attenuation of the irradiance in some spectral ranges. Optical properties of clouds and aerosols as well as the reflection on the Earth's surface also change the spectral irradiance [2]. In addition, absorption and reflection in plant canopies greatly influence the solar spectral irradiance reaching the Earth’s terrestrial surface [3]. The water of oceans, lakes and rivers also modifies the solar spectral irradiance and radiance reaching a target in the water or in shallow areas at the bottom [4, 5, 6, 7].

In many research areas, from photobiology (incl. e.g., photosynthesis, photomorphogenesis, etc.) through atmospheric science to material and chemical sciences, lighting systems of different lamp types and designs are used for experiments (see Supplementary Fig. S1). For example, in the project EDEN-ISS, a greenhouse container in which plants were cultivated using LED lighting was successfully tested in the

Antarctic next to the German Neumayer Station III [8]. The US NASA (National Aeronautics and Space Administration, USA) has been working since the 1950s on how plants can be grown in a spacecraft or a space station to provide the crew with fresh vegetables [9]. Moreover, light therapies by fluorescence tubes have been used successfully for many years to treat various human mental illnesses [10]. In urban areas, indoor and vertical farming will be of great future importance to improve people's food supply and to protect natural resources such as water [11].

When the sun's spectral irradiance reaches an organism, different spectral regions initiate different biological functions. Firstly, photons absorbed by pigments/chromophores can be used as an energy source for photochemical and biological processes such as photosynthesis. Furthermore, the absorption of photons triggers processes such as the circadian rhythm of the metabolism of organisms [12] as well as the control of biological processes in plants [13, 14]. In humans, e.g. the melatonin action spectrum, which has its maximum efficiency around 460 nm, plays an important role as timer for the circadian rhythm [15]. The influence of the sun's spectral irradiance and its temporal and spatial variations have multiple effects on humans, animals, plants and microorganisms, from ecological to cellular level. It has a formative power on the phenotype of organisms, provides the energy for the photochemical conversion of carbon compounds in photosynthetic organisms and has a predisposing effect on interactions in biological communities [16]. Knowledge of the biological effects of solar spectral irradiance (Fig. 1a) in the range from 280-800 nm and especially of the spectral distribution of the irradiance reaching the Earth's surface is, therefore, of great importance in many environmental research areas. Plants are generally sessile organisms and therefore cannot escape changing irradiance in their habitat. In order to recognize the spectral distribution of irradiance and to use it for photochemical and biological processes, plants have evolved many different radiation-absorbing pigments and chromophores integrated in various photoreceptors and photosynthetic systems [11] (Fig. 1b) such as cryptochromes [17], photochromes [18], phototropins [19], phycoerythrin, carotenoids [11] and chlorophyll a and b [20]. With their help, plants and photosynthetically active algae and cyanobacteria convert electromagnetic energy into chemical energy and use their photoreceptors to adapt to temporal and spatial changes of spectral irradiance. This is particularly important in dense vegetation, where competition for light is the main driver for plant development or in suddenly occurring light gaps where gathering information on the irradiance dose and the spectral distribution is an essential measure for plants to respond or adapt to the new conditions or to find a way to improve their situation [21].

A recent study on the influence of green light [22] emphasizes the potential of LED technology for photobiological research. It shows that low irradiance doses of green light are sufficient to induce and maintain the circadian rhythms in thale cress (*Arabidopsisthaliana*) and that cryptochromes contribute to this reaction.

The spectral distribution of the irradiance has major influence on morphological and chemical phenotype (metabolic composition), emission of volatile organic compounds (VOCs), seed germination and flowering time, and shade avoidance and phototropism [16,23. For example, in basil (*Ocimum basilicum*) the irradiance dose ratio at 669 nm (active phytochrome Pfr) to 465 nm (blue light photoreceptor) has a

major influence on plant growth, nutrient content; terpenoid content of leaf glands, and stomata opening [24].

However, many relationships regarding the spectral distribution of irradiance and its effects on plants, humans, animals and materials are still not sufficiently understood. Recently, Zhen and Bugbee (2020) proposed to extend the range of photosynthetically active radiation (PAR), currently defined as 400-700 nm, to 750 nm, as they could demonstrate that photons of this wavelength also contribute to photosynthesis in diverse crop species [25]. Therefore, photobiological research would profit from experiments under environmentally controlled conditions, including a lighting system that is able to simulate natural solar spectral irradiance. Ideally, the lighting system should mimic a multitude of various natural irradiance conditions reflecting the daily and seasonal changes of spectral distribution and irradiance over time.

The invention of LEDs [26] and the development of new LED types, e.g. blue LEDs [27], allow nowadays to design LED lighting systems with a broad spectrum. LEDs have a number of advantages compared to conventional lamps (metal halide lamps, fluorescent tubes, high-pressure sodium lamps). Advantages are their high efficiency in the range of 365-800 nm combined with very long life: 20,000 - 100,000 h depending on LED type and influence factors like thermal management, pollution, mechanical force, electrical parameters, etc. [28, 29]. In addition, LEDs have high temporal stability and the possibility of precise dimming of their radiant flux. Another advantage when implementing LEDs in novel lighting systems is their narrowband spectral irradiance with FWHM (Full Width at Half Maximum) of about 15 nm. Thus, by combining LEDs of different wavelengths, the desired target spectrum - natural or artificial - can be precisely assembled by overlaying the individual spectra.

The goal of this work was to develop and construct an energy-efficient LED-based lighting system with a long lifetime for its use in climate simulation chambers with the following boundary conditions: (i) to simulate the spectral irradiance of the standard reference spectrum ASTM G173-03 and sunny cloudless days in Central Europe (360-800 nm with c. 580 Wm^{-2}) as good as possible on the entire experimental area of one m^2, furthermore, and (ii) the ability to simulate changes of natural spectral irradiance, such as those caused by seasonal and diurnal variations including shading effects caused by clouds and vegetation, (iii) Possibility to integrate the lighting system in the ceiling of the existing climate chamber . We are currently not aware of any LED lighting system that allows all of these variations with the required maximum irradiance, homogeneity, spectral distribution, irradiated area and required distance to the experimental plane that could implement this. In the literature, mostly LED solar simulators for solar cell research or for solar cell tests under laboratory conditions [30, 31, 32, 33, 34, 35, 36] are described. These devices have been developed specifically for certain applications and with their technical possibilities and technical characteristics are not suitable for use as lighting ceilings in climate and phytotron chambers. Overall, we aimed to develop, design and physically characterize a novel LED illumination field from UV-A to the near-infrared (360-950 nm), which paves the way for modern experimental approaches in various fields of photobiological research.

Results

Assembly of natural and artificial spectral irradiance by a mixture of different colored LEDs

The lighting system is based on individual LED spectra (Fig. 1c) with sufficient irradiance levels. As a construction prerequisite, we measured separately the spectra of each LED type in a self-made chamber-like installation (see Supplementary Fig. S2). This installation had an experimental plane of 1 m^2 with walls of highly reflective aluminum sheets [2], minimizing light attenuation. The sensor head of the array radiometer was located 1.6 m below the LED lighting field. The individual spectra (Fig. 1c) of 21 LEDs were recorded at about 70% of the maximal current specified by the LED manufacturers. The spectra of two additional LEDs with central wavelength of 850 nm and 940 nm could not be analyzed due to the array radiometer restrictions. The measurements proved that almost all plant relevant spectral ranges, except ultraviolet-B and short-wave ultraviolet-A radiation (290-340 nm) (Fig. 1b) are covered by the different LEDs with sufficient irradiance levels. Thus, using a combination of different LEDs and irradiance levels photobiological experiments are possible with individual wavelength ranges or in regions where particular photoreceptors are active. For example, the ratio (Pr/Pfr) of phytochrome Pr (inactive form absorbs at 660 nm) to photochrome Pfr (active form, absorbs at 730 nm) triggers photomorphogenic responses [21] and can be adjusted specifically in our system.

Finally, the lighting system comprises 23 different LEDs and enabled to mimic the natural solar spectral irradiance as shown in Fig. 1a. The LED field consists of 81 aluminum core boards on the inner main LED field and 19 aluminum core boards mounted on four small LED fields on the outside (Fig. 2a and Fig. 2b). The software can gradually regulate the current consumption of each LED type, allowing the adjustments of the irradiance in individual wavelength ranges. To define how many different LEDs with which wavelength are required to simulate the solar spectrum, or other target spectrum, as close as possible, we programmed and adapted an algorithm that uses the Lawson-Hanson method [37] 'Non-Negative Least Square'. Using this algorithm, we can calculate the optimal composition of the desired target spectrum using the individual LED spectra as input parameters (Fig. 3d). As an example, Figure 3d depicts the comparison of the target spectrum ASTM G173-03 (standard reference spectrum of the American Society for Testing and Materials: https://www.astm.org/search/fullsite-search.html?query=solar%20spectral%20irradiance&) and the generated spectrum. The simulated spectrum achieved an integrated irradiance of 439 Wm^{-2} in the wavelength range from 400-700 nm (PAR range), which corresponds to a photosynthetic photon flux density (PPFD) of 2,020 µmol m^{-2} s^{-1}. The ASTM G173-03 spectrum has an integrated irradiance of 430 Wm^{-2} in this PAR region, which corresponds to a deviation of 2% of the simulated compared to the target spectrum. Integrated over the range from 360-800 nm, the LED lighting field produces an irradiance of 571 Wm^{-2} compared to 580 W m^{-2} of the ASTM G173-03 spectrum, corresponding to a deviation between both spectra of 1.6%. In the range from 400-500 nm the deviation to ASTM G173-03 was -1.2%, at 500-600 nm -4.3%, at 600-700 nm 0.9% and from 700-800 nm 4.9%, respectively. The integrated irradiance of ASTM G173-03 in the spectral range of 800-1000 nm is

150 W m^{-2}, our system archives in this spectral range a calculated radiant flux of 143 W (see Supplementary Fig. S3).

To calculate the spectral deviation $S_d(\lambda_1,\lambda_2)$ between the ASTM G173-03 and the simulated spectrum the following equation (1) was used with a spectral resolution of 1 nm:

$$S_d(\lambda_1,\lambda_2) = \int_{\lambda_1}^{\lambda_2} \left(\frac{|I_{ASTM\ G173-03}(\lambda) - I_{Simulated}(\lambda)|}{I_{ASTM\ G173-03}(\lambda)}\, d\lambda \right) * 100\% \qquad (1)$$

In the spectral range from 360 nm (λ_1) - 650 nm (λ_2), the new LED lighting field is able to reproduce spectral irradiance of ASTM G173-03with a spectral deviation of 7% on average.

From 650 nm to the near infrared (800 nm) the spectral deviation is slightly higher, about 17%, due to the smaller number of different LEDs installed in this wavelength range. From 360-800 nm the LED lighting system is able to reproduce natural irradiance in its spectral distribution with a spectral deviation of 10%.

In addition to the spectroradiometric measurements, a pyranometer was used to measure the integrated irradiance. Compared to the 729 Wm^{-2}, emitted from the LED lighting field the integrated irradiance of the ASTM is 879 Wm^{-2} (in the spectral range from 300-1,300 nm). The difference can be explained by the missing infrared irradiance, > 950 nm of the LED lighting field. The maximum irradiance achievable by our system is 2,554 Wm^{-2}, though without matching a defined target spectrum (Fig. 6b).

Temporal stability of irradiance of the LED field

To analyze temporal stability of the LED lighting field, we performed seven measurements at 10-minute-intervals during the simulation of the ASTM G173-03 spectrum. The integrated irradiance (300-800 nm) did not change by more than 0.2% during 70 minutes.

Temperature of single LEDs and the complete LED lighting field

The temperature of the active LEDs is one of the main influencing factors [28, 29] regarding lifetime and irradiance maintenance. We measured, therefore, the temperature using two different methods. First, we used a thermocouple cable type K, which was glued as close as possible to the LED housing, second, the temperature was measured with an infrared camera. Both measurements showed, that the temperatures of single LEDs and of the entire LED lighting field did not exceed 40°C during the simulation of the ASTM G173-03 spectrum.

Spatial spectral distribution across the experimental layer of the light system

The previous measurements always referred to a single central point in the measurement plane, but an important aspect for us was how the spectral irradiance was spatially distributed across the entire

experimental space of one m^2. Spatial inhomogeneity is a shortcoming for all light systems in climate and growth chambers. It determines the space within which plants/objects can be exposed under comparable spectral irradiance conditions. To determine the homogeneity of the spectral irradiance we measured the spectral irradiance on a 9x9 point grid with 0.1 m distance.

For the range of 360-800 nm, the averaged ± s.d. irradiance was 556 ± 15 Wm^{-2}. To determine the spectral spatial distribution across the experimental space, five spectral intervals (1-5) were defined (in nm): 360-400, 400-500, 500-600, 600-700 and 700-800, respectively. The mean of the 81 measurements was calculated for the respective wavelength ranges. In order to assess the spectral inhomogeneity in the respective spectral intervals, we then determined the ratio of the value at the xy position divided by the mean value of the total area. Figure 4 shows the inhomogeneity distributions of the irradiance for the spectral intervals. The corresponding histogram is also shown, in which the standard deviation is given as a measure of the scatter in the experimental layer in relation to the specific spectral interval. The evaluation of the spectral distribution of the irradiance and inhomogeneity over the test room is important insofar as this is the only way to ensure that the spectral irradiance is distributed as evenly as possible over the entire experimental area. The results show that in addition to the integrated irradiance from 360-800 nm, the individual spectral ranges are also distributed homogeneously in the experimental layer. On average, the deviations in the area based on the maximum value of the total area were 2.1 % for 360-800 nm, 4.5 % for 360-400 nm, 4.4 % for 400-500 nm, 2.1 % for 500-600 nm, 2.1 % for 600-700 nm and 4.3 % for 700-800 nm, respectively This shows that with the LED lighting field, plants (objects) can be exposed homogeneously on an area of 1 m^2.

Simulation of the spectral irradiance of sunlight in the diurnal course

Due to the diurnal variation of solar elevation and the associated changes in the optical path through the atmosphere, there are changes in both the irradiance and its spectral distribution. In order to show that the new LED lighting field is able to reproduce these diurnal changes of the solar spectrum, its irradiance was compared with the irradiance measured at a sunny day between sunrise and sunset (19 May 2007; 48°13'13.1"N 11°35'51.4"E) (see Supplementary Fig. S5). The diurnal course of integrated irradiance from 360-800 nm is shown in Fig. 5a and compared to a diurnal course generated by the LED lighting field. From the data it is obvious that the new system is able to generate irradiance present in nature. It can be seen that the integrated irradiance from 360-800 nm of the simulated spectra almost entirely overlap with the measured natural spectra at the different hours from midnight to noon, the deviation between the simulated and measured irradiance is smaller than 1.5 % for every time of the day. Moreover, we dissected the simulated spectra in wavebands relevant for the absorption of the different photosynthetic pigments and chromophores (see Fig. 1b) to check whether the LED lighting field is able to simulate diurnal changes in irradiance in wave bands crucial for distinct biological activities and processes. We defined a range from 360-400 nm (e.g. covering the absorption of the UV-A/ blue light photoreceptor) and then in 25 nm intervals from 400-800 nm; in total 17 spectral bands. In Fig. 5b, the diurnal variation of natural solar irradiance is plotted for each of the 17 spectral wave bands, forming a set of curves. As in Fig. 5a, we plotted the calculated values from the LED lighting field in comparison to natural values. In

order to illustrate the comparison of the ratios of natural irradiance to simulated irradiance in the respective spectral range, the curve profiles of the simulated irradiance were set in relation to those of measured irradiance in nature (Fig. 5c). The resulting curves gave an almost horizontal straight line at a ratio of 1 over the entire daily light period. For example, the wavelength range from 475-500 nm shows a deviation of less than 4% over the light phase. Only in the early morning and evening hours shortly before sunrise and sunset, the spectra generated with the LED lighting field deviated somewhat more from natural irradiance because irradiance before sunrise and after sunset is very small (20-33 Wm^{-2} compared to 533 Wm^{-2} at noon).

Simulation of natural spectral irradiance and spectra for horticultural and technical applications

The possible applications of such a lighting system are manifold. We have selected four different scenarios as examples: (i) spectral irradiance conditions in horticultural production systems [38, 39, 40] (Fig. 6a); (ii) high irradiance that might be used for testing aging processes of materials [41, 42] (Fig. 6b); (iii) full bright sunlight on a sunny and cloud free situations [43, 44, 45] (Fig. 6c); (iv) the spectral irradiance environment of understory plants within a tree (birch) canopy [46, 47, 48] (Fig. 6d). Figure 6a exemplifies 'artificial light' (a 365 nm, 450 nm, and 520 nm LED) that may be used in horticultural production systems e.g. in vertical farming or in greenhouses. Other possible applications of such a light system are in materials sciences, where high irradiance (in our case up to 2,500 W m^{-2}), which is more than twice than the maximum irradiance occurring in central Europe [13], is used for aging tests (Fig. 6b) for example. Figure 6c shows the spectrum of a sunny day on May 19th 2007 at 12:18 measured at Helmholtz Zentrum München, compared to the spectrum generated by the LED lighting field. Finally, Fig. 6d compares the spectrum recorded [49] in the shade of a birch tree compared to the simulated spectrum. This show that the lighting system is suitable to simulate different spectra for different applications.

Discussion

The LED Sun Simulater presented here enables the generation of spectra for the exposure of biological samples/organisms and materials in a wavelength range of 360-950 nm. Considering that the radiant flux of each of the 23 individual LEDs can be regulated in 100 levels, theoretically more than 100^{23} different spectra can be generated. In addition, the system produces very high irradiance and reaches or even exceeds irradiance on the Earths' surface. The market for LED-based lamp systems is rapidly growing for plant cultivation in greenhouses [50, 51, 52, 53, 54, 55] and in climate chambers for research purposes on cell cultures and small plants [56, 57, 58]. Usually, these are lamp systems equipped with a few LED types only. The most common lighting devices for horticulture are fluorescent tubes, sodium high-pressure lamps and LEDs. The fluorescent tubes have a PAR efficiency of 1.25 µmol photons s^{-1} W^{-1} (µmol PAR photons per second per Watt of energy), the sodium high-pressure lamps 1.87 µmol photons s^{-1} W^{-1} and LEDs 1.91 µmol photons s^{-1} W^{-1} [56]. However, these standard lighting devices are not comparable with the system presented here, which was built aiming of building up a solar simulator in the spectral range of 360-950 nm with a close match to solar spectral irradiance.

Compared to solar spectral irradiance, it should be noted that the short-wave UV range (290-350 nm) has been excluded from our LED lighting field. This is because LEDs' development for this spectral range has not yet progressed as far as for other wavelengths. The UV-B LEDs, e.g. a 315 nm LED driven with a current of 350 mA and a typical radiant flux of 26 mW, also have an extrapolated L70 lifetime of < 3000 h [59], which is low compared to LEDs in the UV-A (>360 nm) and in the spectral range from 400-950 nm. Integrating the spectral irradiance of ASTM G173-03 from 300-360 nm results in 138 Wm^2. Using UV LEDs, 5307 single LEDs would be necessary to achieve this irradiance in our LED lighting system. For this reason, we have decided not to include this group of LEDs in our setup yet. When selecting the LEDs, we have taken care to use LEDs with the longest possible and comparable lifetime. However, it has been known for a long time that short-wave UV radiation is very important for plants, humans and animals, but also harmful [60]. The UV-B component of solar spectral irradiance reaching the ground (from about 290 nm to 320 nm) is highly variable and varies with the sun's position, the absorption/reflection of clouds, and the dynamics of the atmospheric ozone layer [60]. Action spectra showed early on that organ organisms react to UV-B radiation [61]. This is related to the fact that biomolecules, such as DNA and proteins, absorb UV radiation, leading to mutations in certain genetic material areas [62] and to damage cellular metabolic processes [61]. Recent work shows that plants possess a UV-B photoreceptor [63], which in interaction with chryptochome and phytochromes allows plants to adapt dynamically to the prevailing ‘light climate’ [64]. This shows that the main focus of the further development of our lighting field must be including UV LEDs, if it’s technical achievable. Alternatively, it is possible to supplement the UV-B part of the solar spectral irradiance by a combination of the LED lighting field with two types of conventionally used UV tubes with a peak wavelength of 313 nm and 340 nm. A model for this hybrid system could be the sun simulators (https://www.helmholtz-muenchen.de/eus/facilities/sun-simulators/index.html) available at the Institute [65, 66]. These sun simulators use UV tubes with a peak wavelength of 313 nm and special borosilicate and lime glass filters to shape the spectral irradiance close to the solar spectrum. By replacing the previous lamps (blue fluorescent tubes and metal halide and halogen lamps) [65, 66] with the LED lighting field described here, while retaining the 313 nm UV fluorescent tubes plus adding 340 nm tubes, a hybrid sun simulator can be developed with a spectral irradiance very close to the solar spectrum from 280-950 nm. If there is a scientific reason to increase the infrared irradiance beyond 950 nm, we suggest implementing additional halogen lamps. They produce infrared irradiance more efficient than LEDs. Such a hybrid sun simulator, including UV tubes, LEDs, and halogen lamps, could probably simulate a solar spectrum from 280-2500 nm.

The described LED lighting field delivers all photons in the spectral range (350-800 nm) important for plants [67] in sufficient quantity and in a balanced mixing ratio for the activation and regulation of photoreceptors (UV-A and blue light receptor, phytochrome system Fr / Pfr; except for the UV-B receptor;) as well as for the photochemical energy conversion of the photosynthesis (carotenoids, xanthophylls, and chlorophylls). The new system allows, therefore, specifically to manipulate the photobiological behavior of plants. The possibility of adjusting the ratio of UV-A / blue light to red- and near IR, in front of a natural PAR background, could be one of the outstanding features that this LED system achieves.

The absorption of photons is always associated with the transfer of thermal energy. If leaves/surfaces are irradiated they heat up [68]. However, leaf temperatures are not constant. They fluctuate in high frequency due to short-term changes in irradiance and rapid leaf movements due to fluctuation wind eddies [69]. Leaf surface temperature is almost always different from ambient air temperature. In full bright sunlight leaf temperature is usually slightly higher, while in the shade leaf temperatures can be lower than the surrounding air temperature [70]. Leaves adapt their temperature by evaporation of water through their stomata and cool down [71] depending on within plant water availability. In addition to ambient air temperature, relative humidity, and leaf morphology [72], the spectral irradiance has a decisive effect on the leaf temperature. Near and far IR (> 850 nm) of the solar spectrum is perceived by plants only as thermal radiation (absorption by water molecules, CO_2, lignin) and has no direct physiological effect according to current knowledge. However, the different leaf temperatures in the absence of near IR may lead to indirect physiological effects. With increasing wavelength, the proportion of reflection increases in plants [73] and, depending on the physiological state, and leaf morphology in the IR band amounts to c. 60%. These characteristic reflection properties of leaves are exploited in remote sensing to differentiate vegetation elements and derive physiological states (e.g. drought, senescence) from satellite data [74].

Conventional lighting systems in climatic chambers and greenhouses have a high proportion of long wave radiation, which leads to a strong non-natural thermal gradient within the plant canopy and heating of shoot tips. In order to counteract this thermal gradient, climate chambers and greenhouses with additional lighting must be strongly cooled and ventilated, which means that either relatively cold air is blown in or the air exchange rate is very high. Both can lead to very heterogeneous environmental conditions for the plants.

LED lighting fields such as the one presented here make it possible to cultivate plants under a ‘colder’ irradiance, but at the same time to apply the spectral irradiance that is important for physiological and morphological processes in natural doses without overheating the upper plant parts or causing mechanical stress through air movement. At the same time, the energy requirement of the system is reduced due to the better electrical power efficiency of the LEDs and the low required cooling capacity of the climate chambers and greenhouse cabins. The LED lighting field we constructed is designed for a possible irradiance in the IR up to c. 950 nm. This means that far less IR is available than is contained in the solar spectrum, but it allows plants to be attracted under a ‘warmer’ light beyond 800 nm that can be used in a controlled manner.

Using the same concept, a true large-scale LED solar simulator could be realized by increasing the number of the main LED field. The low working temperature (40°C) of the LED lighting field will increase the reliability, lifetime, efficiency, and irradiance maintenance.

In summary, our development of a lighting field based on LED technology paves the way into future applications ranging from photobiology to materials research, even if it is not feasible yet, to simulate solar spectral irradiance from 290-2500 nm efficient solely with LEDs only. The LED Sun Simulator

presented here, which can homogeneously simulate different spectra - from solar to artificial - from UV-A (360 nm) to the near IR (950 nm) over an area of 1 m^{-2}, however, represents an important milestone in this direction.

Materials And Methods

Selection of appropriate LEDs for the lighting field

The spectral irradiance throughout this study was measured with an array radiometer (Newport OSM400, Newport Spectra-Physics GmbH, Darmstadt, Germany with a UV/VIS range from 200-800 nm, spectral resolution of 1 nm, a Sony CCD-Sensor with 2046 pixel, and a slit with of 50 µm). From individual LED spectra by superimposing the individual LED spectra $LED_i(\lambda)$ a desired target spectrum can be simulated as a linear combination of individual spectra multiplied with a proportion coefficient x_i (equation (2)). The number of x_i and $LED_i(\lambda)$ is depending on how many individual LED spectra are present; in this work the number is restricted to 23, i = 1, . . . , 23. The desired target spectrum can be arbitrary depending on the experimental application, for example the solar spectrum at a certain time or solar zenith angle or at the floor of a dense forest canopy. The simulated spectrum $S_{simulated}$ results by the following equation (2):

$$S_{simulated}(\lambda) = \sum_{i=1}^{n} x_i LED_i(\lambda) \quad \left[\frac{W}{m^2 nm}\right] \qquad (2)$$

How the proportion coefficients x_i were determined will be explained in the subsection ‘Non-negative least squares for solving multi coefficient linear regression’ (see below). As prerequisite for the calculations, a market research was conducted to determine which LEDs with a certain wavelength and sufficient radiant power are commercially available. The list of the selected ‘high power’ LEDs is given in the Supplementary Information (Table S1). The Sunlike LED™ from Seoul Semiconductor (Seoul Semiconductor Europe GmbH, Munich, Germany) is a so-called ‘white’ LED with a wide emission spectrum, which provides the basic irradiance for the new lighting system.

‘White’ LEDs produce their emission spectrum in the following way: A blue LED with an emission of c. 450 nm excites a mixture of fluorescent substances by its short-wave emitted spectrum. Depending on the composition of the fluorochromes, this mixture emits lower-energy wavelengths in various spectral ranges and thus generates ‘white’ light [75]. The special feature of the Sunlike LED™ is that - compared to conventional ‘white’ LEDs - the excitation of the light source is done by means of an ultraviolet LED with a wavelength of c. 405-420 nm and a special combination of fluorescent materials. This results in a ‘white’ spectrum that radiates a sufficiently high power in this spectral range already from a wavelength of 420 nm.

The phosphor composition of the Sunlike LED ensures a relatively uniform radiation in the range of 420-700 nm. By using such a ‘white’ LED as backbone of the lighting system, the total number of required

LEDs could be significantly reduced. Manufacturers of 'white' LEDs express the radiated power in lumen in their data sheets, and in most cases the standardized spectral distribution is also given in the form of a graph. For the present work, overall, the curves of 23 LED emissions, as specified by the manufacturers, were digitized by software (Engauge Digitizer Version 10.11) or approximated by a Gaussian distribution. These spectra were then used further for our calculations.

For the first basic calculations, which were necessary for the selection of the different LEDs, it was sufficient to represent the emission spectra of the different LEDs by digitized spectral distribution or by Gaussian distribution. In most data sheets of the LED manufacturers the following parameters are given: The typical dominant wavelength, the spectral bandwidth (FWHM) and the radiant flux (R) All these specifications are only typical values and vary depending on the binning (grouping of LED parameters) of the LEDs. For a homogenous distribution of radiation, only LEDs with a beam angle of more than 110° were used.

For many LEDs emitting in the visible range (400-700 nm), the radiant power is specified in the data sheet in the unit lumen. For further calculations it was therefore necessary to convert from lumen to W.

With the help of the parameterization of all LED specifics, it was now possible to calculate the required number of individual LEDs using an algorithm to synthesize the desired target spectrum (e.g. Fig. 3). To find the optimal parameters x_i a special algorithm was applied (see next section).

Later on, this algorithm was applied to synthesize a target spectrum by using the measured individual LED spectra (Fig. 1c)

Non-negative least squares for solving multi coefficient linear regression

In the present work, the algorithm was programmed with R v3.5.1 (R Core Team, 2018), which includes the package 'nnls'. This nnls-package (non-negative least squares) is an implementation of Lawson-Hanson NNLS (Lawson and Hanson, 1995) to solve the problem min $|| Ax - b ||_2$ with the constraint $x \geq 0$ where $x \in R^n$, $b \in R^m$ and A is a m by n matrix.

In this work, the vector b_i , i = 1, . . . , m, represent the target spectrum $S_{target}(\lambda)$ [$Wm^{-2}nm^{-1}$] , b_1 is the target spectrum S_{target}(280 nm) and b_2 S_{target}(281 nm) until $b_{1,020}$ S_{target}(1300 nm) in 1 nm units. L11 to Lm1 is the spectral distribution of $LED_1(\lambda)$ [$Wm^{-2}nm^{-1}$], in the range of 280 nm - 1300 nm in 1 nm units, L11 to L1n are the n-LED(λ) [$Wm^{-2}nm^{-1}$], in this work the number of n, the number of individual LED types, is restricted to 23. This results in a linear regression model (equation (3)) with *r* a n-vector of residual and *x* a n-vector of calculated coefficients.

$$\begin{pmatrix} b_1 \\ \vdots \\ b_m \end{pmatrix} = \left(\begin{pmatrix} L11 & \cdots & L1n \\ \vdots & \ddots & \vdots \\ Lm1 & \cdots & Lmn \end{pmatrix} \begin{pmatrix} x_1 \\ \vdots \\ x_n \end{pmatrix} + r \right) \qquad (3)$$

Cooling system

The calculations revealed that a very high density of LEDs and / or a high power of LEDs is required to achieve an integrated irradiance (360-800 nm) of about 580 Wm^{-2} at a distance of 1.6 meter. The LED irradiance describes the part of the energy that is radiated in form of electromagnetic waves. The biggest part of the rest energy (depending on the efficiency of the individual LED types) will be released by thermal conduction and thermal convection. This means that for an LED-based lighting system, with such a high irradiance, the LEDs must be equipped with a very efficient cooling system. The main cooling part of our system became realized by an in-house developed and constructed 18 kg active, water-cooled heat sink (see Supplementary Fig. S4g). The heat sink is made of aluminum due to its good thermal conductivity of 220 $W\ K^{-1}\ m^{-2}$ (76Kuchling 2014 in die ref). With a size of 53 cm x 53 cm the heat sink offers space for 81 circuit boards and their cabling (see Supplementary Fig. S4a).

LED-drivers and control unit

A small change in voltage at the LED leads to a large change in current. For this reason, electronic ballasts designed as constant current sources were used for this work. For the operation of the LED circuit boards, described above, a constant current ballast is required. Depending on the composition of the LED circuit board and the number and type of LEDs, a ballast must be selected that supplies the required forward voltage of the LEDs connected in series as well as the required current. Six different ballasts were used (see Supplementary Table S1).

The ballasts have an open-circuit, short-circuit and overtemperature shutdown as protective functions. According to the manufacturers' protocol, they have a life of more than 50,000 h at a housing temperature below 75°C. A very important aspect that these ballasts fulfil is the control of the LED radiation intensity, not by pulse width modulation (PWM), but by controlling the current intensity. Regardless of whether the dimming signal is sent to the ballasts via the DALI interface or via 0-10V, the dimming behavior or the change in current intensity is linear to the dimming signal. However, each output of the constant current ballast (LED driver) has a specific AC component, this is called 'ripple' and is specified for these ballasts at less than 5%. Own measurements with an oscilloscope have shown that the residual ripple at 60% load is < 2%. The frequency of the alternating current component is in the range above 2 kHz. Such ripples can be considered as small compared to traditional light sources operated by alternating voltage [79]. The supply voltage of the ballasts is realized via the 230 V AC mains

The lighting control system DALI (Digital Addressable Lighting Interface, industry-standardized protocol, specified in IEC 62386) is a serial bus system based on two lines for controlling lamps. The DALI system is part of IEC 62386, which defines a standard protocol for communication between lamps, sensors and ballasts. The controller / master sends a 16 bit Manchester code, the ballasts respond with an 8 bit Manchester code. A controller / master can control up to 64 ballasts on the two-line serial bus. It is also possible to use several masters and increase the number of digitally addressable ballasts. In this thesis a controller was used which contain four masters and thus control 256 ballasts individually. One DALI line

allows the management of 16 different groups and 16 different scenes. A scene contains up to 64 different ballasts and a specific dimming level for each ballast [77]

Assembly of circuid boards

In order to operate the large number of LEDs required for this lighting system, we arranged them in a series connection. When the LEDs are connected in series, the individual forward voltages add up to a total voltage which is applied to the series connection. However, the current is the same for each LED and thus typically also the radiated power. Since practically all 'monochromatic' high-power LEDs are SMD (Surface Mounted Device), it was necessary to develop a printed circuit board (PCB) on which the LEDs can be soldered and connected in series (see Supplementary Fig. S4 d, e, f). Three different PCBs or layouts were developed for this purpose using the AUTODESK-EAGLE version 9.4.1 software (AUTODESK, San Rafael, USA). Common to all layouts is that the LEDs are symmetrically arranged in a small space and connected in series. In order to keep the ohmic losses on the boards as low as possible, the copper track thickness was chosen to be 105 µm and the width of the individual connections of the LEDs from the cathode to the anode, the next LED, was increased to the width of the LEDs. The base material of the circuit boards is 1.6 mm thick aluminium. A thin layer / foil of dielectric was applied to this aluminium. Then the copper conductor paths, the copper thermal pads for the LEDs and the pads for the anode and cathode were applied. A white solder resist prevented the solder from running during the soldering process and still acts as a reflective surface when used as a light-engine.

After the production of the circuit boards the soldering paste was applied exactly to the solder pads of anodes and cathodes with a stencil. The LEDs were mounted and soldered in a plasma SMD soldering process, the production of the PCBs and the mounting and soldering of the LEDs was done by an outside company.

The number of LEDs connected in series depends on the LED drivers used. These have a defined voltage range in which they can supply the LEDs with constant current. For the developed LED light system 5 different designs for the circuit boards were developed (see Supplementary Fig.4 b, c, d, e, f). For the high power SMD LEDs with a footprint of 3.3 x 3.3 mm, 56 LEDs were connected in series on a PCB (see Supplementary Fig. S4d). For LEDs with a footprint of 2.7 x 2.7 mm a special layout with 56 LEDs connected in series on a PCB (see Supplementary Fig. S4e). In case of SMD LEDs with a footprint of 5x6 mm, 36 LEDs were connected in series also on a special PCB layout (see Supplementary Fig. S4f).

Declarations

Acknowledgements

We thank the technical staff of EUS for their help during the construction of the LED lighting field.

Author Contributions Statement

GS, AA and JPS conceived and designed the work with help from JBW and AG. AK with help from PK and MO constructed the LED lighting field. AK designed and developed the LED Sun Simulator and performed spectral radiometric measurements and developed the statistical tools and analyzed the data. AA provided diurnal spectral radiometric data from HMGU Campus. AK wrote the first draft of the manuscript with the help of GS and JPS. All authors contributed to the interpretation of the findings and edited and approved the manuscript.

Competing financial interests

The authors declare no competing financial interests.

References

1. Steinhilber, F., Beer, J. & Fröhlich, C. Total solar irradiance during the Holocene. *Geophys. Res. Lett.***36** (2009).
2. Seckmeyer, G. Simulation der Globalstrahlung für Pflanzenversuche (1991).
3. Reitmayer, H., Werner, H. & Fabian, P. A novel system for spectral analysis of solar radiation within a mixed beech-spruce stand. *Plant Biol.***4**, 228-233 (2002).
4. Théry, M. Forest light and its influence on habitat selection, *Plant Ecol.***153**: 251–261 (2001)
5. Cruz, S., Calado, R., Serodio, J. & Cartaxana, P. Crawling leaves: photosynthesis in sacoglossan sea slugs. *J. Exp. Bot.***64**, 3999-4009 (2013).
6. Shaw, P. J. & Purdie, D. A. Phytoplankton photosynthesis-irradiance parameters in the near-shore UK coastal waters of the North Sea: temporal variation and environmental control. *Mar. Ecol. Prog. Seri.***216**, 83-94 (2001).
7. Gerringa, L. J., Rijkenberg, M. J., Timmermans, R. & Buma, A. G. The influence of solar ultraviolet radiation on the photochemical production of H_2O_2 in the equatorial Atlantic ocean. *J. Sea Res.***51**, 3-10 (2004).
8. Maiwald, V. *et al.* From ice to space: a greenhouse design for Moon or Mars based on a prototype deployed in Antarctica. *CEAS Space J.*, 10.1007/s12567-020-00318-4 (2020).
9. Wheeler, R. M. Agriculture for space: people and places paving the way. *Open Agric.***2**, 14–32 (2017).
10. Tseng, P. T. *et al.* Light therapy in the treatment of patients with bipolar depression: A meta-analytic study. *Eur. Neuropsychopharmacol.***26**, 1037-1047 (2016).
11. Pattison, P. M., Tsao, J. Y., Brainard, G. C. & Bugbee, B. LEDs for photons, physiology and food. *Nature***563**, 493-500 (2018).
12. Wirz-Justice, A. The implications of chronobiology for psychiatry. *Psychiatric. Times***28**, 56-61 (2011).
13. Hogewoning, S. W., Douwstra, P., Trouwborst, G., van Ieperen, W. & Harbinson, J. An artificial solar spectrum substantially alters plant development compared with usual climate room irradiance spectra. *J. Exp. Bot.***61**, 1267-1276 (2010).

14. Jiao, Y., Lau, O. S. & Deng, X. W. Light-regulated transcriptional networks in higher plants. *Nat. Rev. Genet.***8**, 217-230 (2007).
15. Brainard, G. C. *et al.* Action spectrum for melatonin regulation in humans: evidence for a novel circadian photoreceptor. *J. Neurosci.***21**, 6405-6412 (2001).
16. Carvalho, S. D. & Castillo, J. A. Influence of light on plant-phyllosphere interaction. *Front. Plant Sci.***9**, 1482, 10.3389/fpls.2018.01482 (2018).
17. Ahmad, M. *et al.* Action spectrum for cryptochrome-dependent hypocotyl growth inhibition in Arabidopsis. *Plant Physiol.***129**, 774-785 (2002).
18. Fankhauser, C. The phytochromes, a family of red/far-red absorbing photoreceptors. *J. Biol. Chem.***276**, 11453-11456 (2001).
19. Briggs, W. R. & Christie, J. M. Phototropins 1 and 2: versatile plant blue-light receptors. *Trends Plant Sci.***7**, 204-210 (2002).
20. Atwell, B. J., Kriedemann, P. E. & Turnbull, C. G. *Plants in action: adaptation in nature, performance in cultivation*. (Macmillan Education AU, 1999).
21. Pierik, R., Mommer, L., Voesenek, L. A. C. J. & Robinson, D. Molecular mechanisms of plant competition: neighbour detection and response strategies. *Funct. Ecol.***27**, 841-853 (2013).
22. Battle, M. W. & Jones, M. A. Cryptochromes integrate green light signals into the circadian system. *Plant Cell Environ.***43**, 16-27 (2020).
23. de Wit, M., Galvao, V. C. & Fankhauser, C. Light-mediated hormonal regulation of plant growth and development. *Annu. Rev. Plant Biol.***67**, 513-537 (2016).
24. Pennisi, G. *et al.* Unraveling the role of red:blue LED lights on resource use efficiency and nutritional properties of indoor grown sweet Basil. *Front. Plant Sci.***10**, 305, 10.3389/fpls.2019.00305 (2019).
25. Zhen, S. & Bugbee, B. Far-red photons have equivalent efficiency to traditional photosynthetic photons: implications for re-defining photosynthetically active radiation. *Plant Cell Environ.*, 10.1111/pce.13730 (2020).
26. Holonyak, N. & Bevacqua, S. F. Coherent (visible) light emission from Ga(As1−xPx) junctions. *Appl. Phys. Lett.***1**, 82-83, 10.1063/1.1753706 (1962).
27. Nakamura, S. Nobel Prize 2014: Akasaki, Amano & Nakamura. *Nat Phys***10**, 791-791 (2014).
28. Osram. Reliability and lifetime of LEDs. *Application Note No*. AN006 (2020).
29. CREE. *APPLICATION NOTE* CLD-AP57 REV 66 (2020).
30. Kohraku, S. & Kurokawa, K. A fundamental experiment for discrete-wavelength LED solar simulator. *Sol. Energy mater. Sol. Cells***90**, 3364-3370 (2006).
31. Kohraku, S. & Kurokawa, K. New methods for solar cells measurement by LED solar simulator *3rd World Conference on Photovoltaic Energy Conversion* **2**, 1977-1980 (2003).
32. Al-Ahmad, A. Y. *et al.* Modular LED arrays for large area solar simulation. *Prog. Photovoltaics***27**, 179-189 (2019).

33. Linden, K. J., Neal, W. R. & Serreze, H. B. Adjustable spectrum LED solar simulator *Proc. SPIE* 9003 (2014)
34. Novičkovas, A., Baguckis, A., Vaitkūnas, A., Mekys, A. & Tamošiūnas, V. Investigation of solar simulator based on high-power light-emitting diodes. *Lith. J. Phys.***54**, 114-119 (2014).
35. Kolberg, D., Schubert, F., Klameth, K. & Spinner, D. M. Homogeneity and lifetime performance of a tunable close match LED solar simulator. *Energy Procedia***27**, 306-311 (2012).
36. Kolberg, D., Schubert, F., Lontke, N., Zwigart, A. & Spinner, D. M. Development of tunable close match LED solar simulator with extended spectral range to UV and IR. *Energy Procedia***8**, 100-105 (2011).
37. Lawson, C. L. & Hanson, R. J. *Solving least squares problems*. (SIAM, 1995).
38. He, D., Kozai, T., Niu, G. & Zhang, X. *Light-Emitting DiodesSolid State Lighting Technology and Application Series*, 513-547 (2019).
39. Joshi, N. C. *et al.* Effects of daytime intra-canopy LED illumination on photosynthesis and productivity of bell pepper grown in protected cultivation. *Sci. Horti.***250**, 81-88 (2019).
40. Zhang, Y., Wang, X. R. & Chen, J. Effects of light quality and photoperiod of light emitting LED on growth and biomass accumulation of shallot. *J. Hortic. For.***11**, 78-83 (2019).
41. Wang, Z. *et al.* High irradiance performance of metal halide perovskites for concentrator photovoltaics. *Nat. Energy***3**, 855-861, (2018).
42. Masili, M. & Ventura, L. Equivalence between solar irradiance and solar simulators in aging tests of sunglasses. *Biomed. Eng. Online***15**, 86, 10.1186/s12938-016-0209-7 (2016).
43. Eisenberg, M. J., Habib, B., Alcaraz, M., Thombs, B. D. & Filion, K. B. Bright light therapy for depressive symptoms in hospitalized cardiac patients: A randomized controlled pilot trial. *PLoS One***15**, e0230839, 10.1371/journal.pone.0230839 (2020).
44. Narla, S., Kohli, I., Hamzavi, I. H. & Lim, H. W. Visible light in photodermatology. *Photochem. Photobiol. Sci.***19**, 99-104 (2020).
45. Volf, C. *et al.* Dynamic LED light versus static LED light for depressed inpatients: results from a randomized feasibility trial. *Pilot Feasibility Stud.***6**, 5, 10.1186/s40814-019-0548-9 (2020).
46. Salter, M. G., Franklin, K. A. & Whitelam, G. C. Gating of the rapid shade-avoidance response by the circadian clock in plants. *Nature***426**, 680-683 (2003).
47. Crocco, C. D. *et al.* The transcriptional regulator BBX24 impairs DELLA activity to promote shade avoidance in Arabidopsis thaliana. *Nat. Commun.***6**, 6202, 10.1038/ncomms7202 (2015).
48. Fraser, D. P., Hayes, S. & Franklin, K. A. Photoreceptor crosstalk in shade avoidance. *Curr. Opin. Plant Biol.***33**, 1-7 (2016).
49. Aphalo, Pedro J. The r4photobiology suite. *UV4Plants Bulletin*, **2015**, 21-29, doi:10.19232/uv4pb.2015.1.14(2015)
50. Jiang, J., Mohagheghi, A. & Moallem, M. Energy-Efficient Supplemental LED lighting control for a proof-of-concept greenhouse system. *IEEE Trans. Ind. Electron.***67**, 3033-3042 (2020).

51. Choong, T. W., He, J., Qin, L. & Lee, S. K. Quality of supplementary LED lighting effects on growth and photosynthesis of two different Lactuca recombinant inbred lines (RILs) grown in a tropical greenhouse. *Photosynthetica***56**, 1278-1286 (2018).
52. He, F., Zeng, L., Li, D. & Ren, Z. Study of LED array fill light based on parallel particle swarm optimization in greenhouse planting. *Inf. Proc. Agric.***6**, 73-80 (2019).
53. Nelson, J. A. & Bugbee, B. Analysis of environmental effects on leaf temperature under sunlight, high pressure sodium and light emitting diodes. *PloS one***10**, e0138930 (2015).
54. Cocetta, G. *et al.* Light use efficiency for vegetables production in protected and indoor environments. *Eur. Phys. J. Plus***132**, 10.1140/epjp/i2017-11298-x (2017).
55. Gómez, C. & Gennaro Izzo, L. Increasing efficiency of crop production with LEDs. *AIMS Agric. Food***3**, 135-153 (2018).
56. Blanken, W., Cuaresma, M., Wijffels, R. H. & Janssen, M. Cultivation of microalgae on artificial light comes at a cost. *Algal Res.***2**, 333-340 (2013).
57. Massa, G. D., Wheeler, R. M., Morrow, R. C. & Levine, H. G. Growth chambers on the International Space Station for large plants *VIII International Symposium on Light in Horticulture 1134.* 215-222 (2016).
58. Watson, A. *et al.* Speed breeding is a powerful tool to accelerate crop research and breeding. *Nat. Plants***4**, 23-29, (2018).
59. Knauer, A. *et al.* High power UVB light emitting diodes with optimized n-AlGaN contact layers. *Jpn. J. App. Phys.***58**, 10.7567/1347-4065/ab0f13 (2019).
60. Paul, N. D. & Gwynn-Jones, D. Ecological roles of solar UV radiation: towards an integrated approach. *Trends Ecol. Evol.***18**, 48-55 (2003).
61. Caldwell, M. M., Camp, L. B., Warner, C. W. & Flint, S. D. *Stratospheric ozone reduction, solar ultraviolet radiation and plant life* 87-111 (Springer Berlin Heidelberg, 1986).
62. Willing, E.-M. *et al.* UVR2 ensures transgenerational genome stability under simulated natural UV-B in Arabidopsis t haliana. *Nat. Commun.***7**, 13522, 10.1038/ncomms13522 (2016).
63. Liao, X., Liu, W., Yang, H.-Q. & Jenkins, G. I. A dynamic model of UVR8 photoreceptor signalling in UV-B-acclimated Arabidopsis. *New Phytol.* , 10.1111/nph.16581(2020).
64. Tissot, N. & Ulm, R. Cryptochrome-mediated blue-light signalling modulates UVR8 photoreceptor activity and contributes to UV-B tolerance in Arabidopsis. *Nat. Commun.***11**, 1323, 10.1038/s41467-020-15133-y (2020).
65. Seckmeyer, G. & Payer, H.-D. A new sunlight simulator for ecological research on plants. *J. Photochem. Photobiol. B, Biol.***21**, 175-181 (1993).
66. Thiel, S. *et al.* A Phytotron for Plant Stress Research: How far can artificial lighting compare to natural sunlight?. *J. Plant Physiol.***148**, 456-463,(1996).
67. Sullivan, J. A. & Deng, X. W. From seed to seed: the role of photoreceptors in Arabidopsis development. *Dev. biol.***260**, 289-297 (2003).

68. Monson, R. K. *et al.* High productivity in hybrid-poplar plantations without isoprene emission to the atmosphere. *Proc. Natl. Acad. Sci.***117**, 1596-1605 (2020).
69. Singsaas, E. L. *et al.* Kinetics of leaf temperature fluctuation affect isoprene emission from red oak (Quercus rubra) leaves. *Tree Physiol.***19**, 917-924, (1999).
70. Curtis, O. F. Leaf temperatures and the cooling of leaves by radiation. *Plant Physiology***11**, 343 (1936).
71. Lin, H., Chen, Y., Zhang, H., Fu, P. & Fan, Z. Stronger cooling effects of transpiration and leaf physical traits of plants from a hot dry habitat than from a hot wet habitat. *Funct. Ecol.***31**, 2202-2211 (2017).
72. Tian, M., Yu, G., He, N. & Hou, J. Leaf morphological and anatomical traits from tropical to temperate coniferous forests: Mechanisms and influencing factors. *Sci. Rep.***6**, 19703, 10.1038/srep19703 (2016).
73. Nelson, J. A. & Bugbee, B. Economic analysis of greenhouse lighting: light emitting diodes vs. high intensity discharge fixtures. *PLoS One***9**, e99010, 10.1371/journal.pone.0099010 (2014).
74. Herrmann, I. *et al.* LAI assessment of wheat and potato crops by VENμS and Sentinel-2 bands. *Remote Sens. Environ.***115**, 2141-2151 (2011).
75. Tsao, J. Y. *et al.* Toward smart and ultra-efficient solid-state lighting. *Adv. Opt. Mater.***2**, 809-836 (2014).
76. Kuchling, H. *Taschenbuch der Physik*. Vol. 17 (Fachbuchverl., 1994).
77. Microchip, Digitally Addressable Lighting Interface (DALI) communication. *application note* AN1465 (2012).
78. Hofmann M., Seckmeyer G.: Influence of various irradiance models and their combination on simulation results of photovoltaic systems, *Energies* **2017**, 10, 1495; doi: 10.3390/en10101495, (2017)
79. Seckmeyer G.; Payer H.D.: Lichtschwankungen von wechselstrombetriebenen Lampen, Gartenbauwissenschaft, 53 (4), pp 188 - 191, (1988)

Supplemental Information

Supplemental Figure S1 Different applications for a LED-based solar simulator.

Supplemental Figure S2 Setup of the experimental chamber and the prototype of the LED lighting field. Chamber with a ground area of one m^2 and a distance to the LED lighting field of 1.6 meter. For the side walls of the chamber a high reflective aluminium where used.

Supplemental Figure S3 Normalized spectra of the 810 nm LED (19), 850 nm LED (22) and the 940 nm LED (23). The data were taken from the manufacture datasheets. The typical radiant flux of a single 810 nm LED is 0.52 W@800 mA, 25 °C. In the system are 108 LEDs (810 nm) integrated, which results to a radiant flux of 56 W. For the single 850 nm and 940 nm LED, the typical radiant flux is also about 0.52 W. In the system are 112 LEDs (850 nm) and 56 LEDs (940 nm) integrated. These results of an overall

radiant flux of 58 W for the 850 nm LEDs and 29 W for the 940 nm LEDs. The sum of the overall radiant flux of the 810 nm, 850 nm and the 940 nm LEDs is 143 Watt.

Supplemental Figure S4 Set up of the inner LED lighting field. (a) Picture of the inner LED lighting field, where 81 circuit boards are mounted. (b) Circuit board for the main 'white' LED (Seoul Semiconductor SAWS1566A), four COB (Chip On Board) LED connected in series (c) Circuit board for the 2nd 'white' LED. (d) Circuit board for 56 SMD (Surface Mounted Device) LEDs with a foot print of 2.7x2.7 mm. (e) Circuit board for 56 SMD LEDs with the foot print of 3x3.3 mm. (f) Light engine for 36 SMD LEDs with the foot print of 6x5 mm. (g) Exploded assembly drawing of the inner LED lighting field.

Supplemental Figure S5 Measured natural diurnal solar spectra (19 May 2007; 48°13'13.1"N 11°35'51.4"E from 05:20 to 12:18 CET, Bentham Double-Monochromators) versus the corresponding synthesized LED spectra.

Supplementary Data

Table S1. Six different LED drivers

Table S2: Table of the used LEDs

Figures

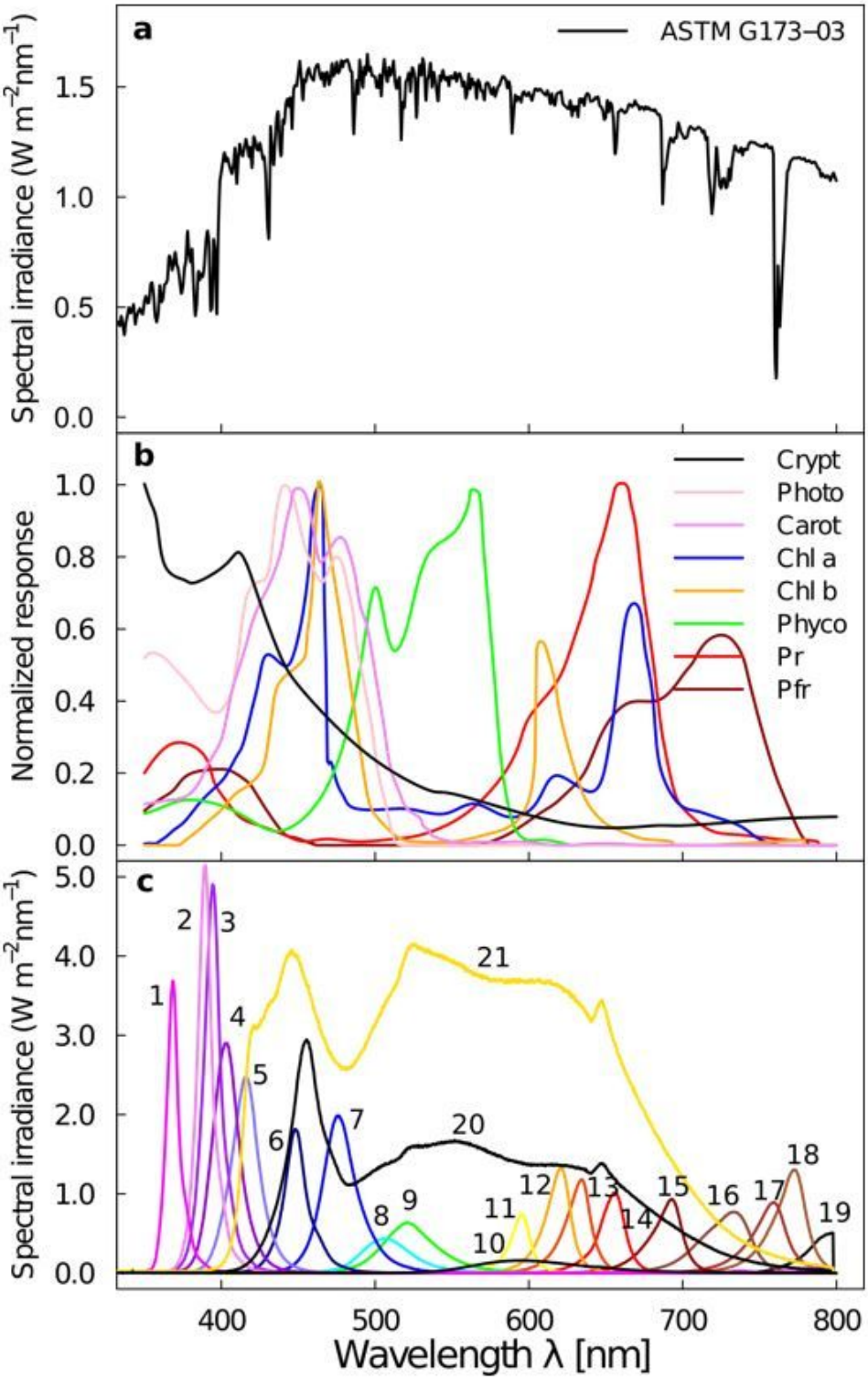

Figure 1

Standard reference solar spectrum, plant action spectra and measured individual spectra LEDs selected for the present lighting field. (a) ASTM G173-03 standard reference spectrum of the American Society for Testing and Materials including the direct and circumsolar irradiance. (b) Plant action spectra, cryptochromes, carotenoids, phototropins, chlorophyll b, phycoerythrin, chlorophyll a, photochromes Pr, and phytochromes Pfr. (c) Measured LED spectra at a distance of 1.6 meter, with the following peak

wavelength (nm): 1 = 365, 2 = 385, 3 = 395, 4 = 405, 5 = 416, 6 = 450, 7 = 475, 8 = 506, 9 = 520, 10 = 590, 11 = 595, 12 = 620, 13 = 633, 14 = 655, 15 = 690, 16 = 733, 17 = 760, 18 = 770, 19 = 810. Additionally, two types of ‘white’ LEDs 20 and 21.

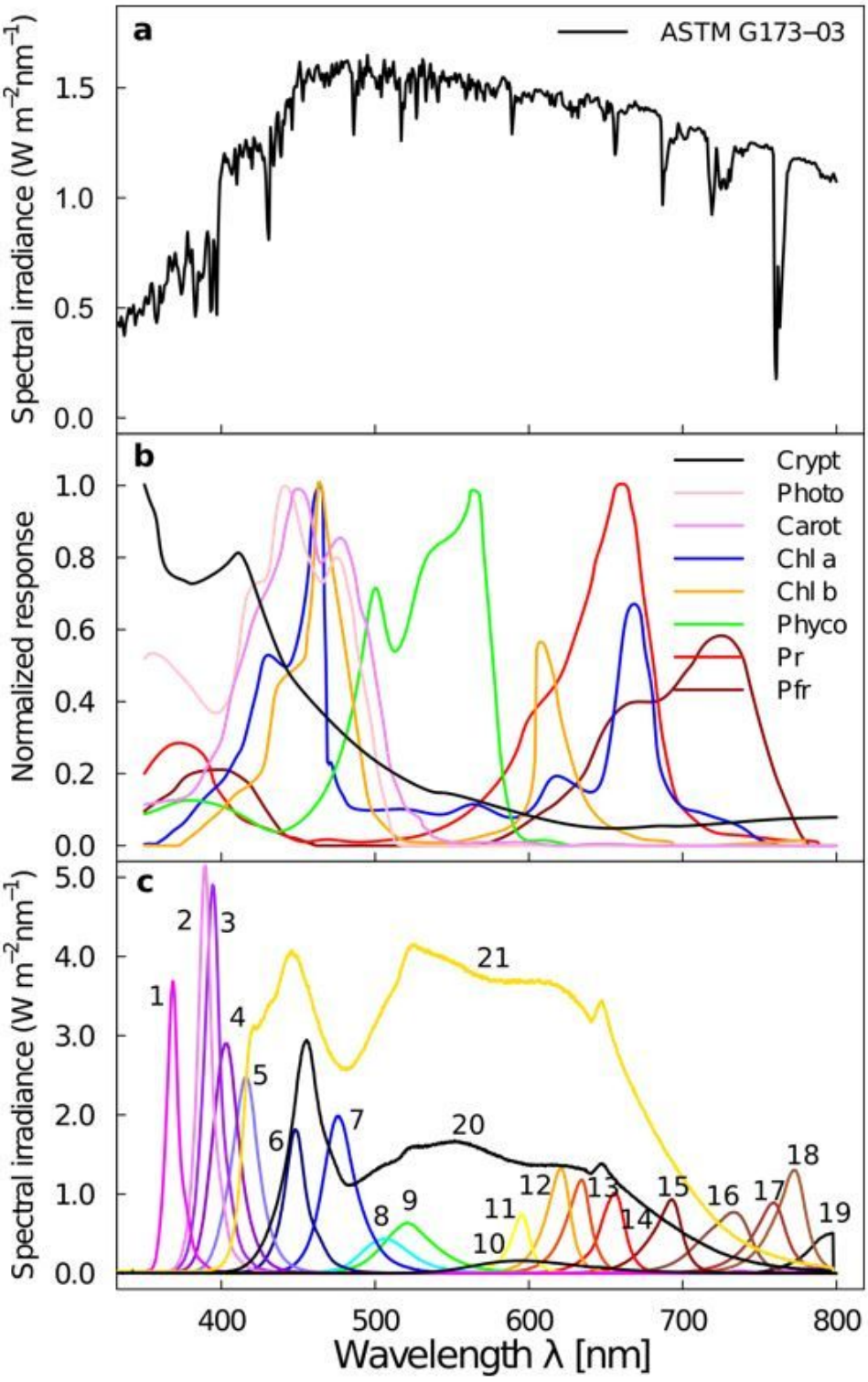

Figure 1

Standard reference solar spectrum, plant action spectra and measured individual spectra LEDs selected for the present lighting field. (a) ASTM G173-03 standard reference spectrum of the American Society for

Testing and Materials including the direct and circumsolar irradiance. (b) Plant action spectra, cryptochromes, carotenoids, phototropins, chlorophyll b, phycoerythrin, chlorophyll a, photochromes Pr, and phytochromes Pfr. (c) Measured LED spectra at a distance of 1.6 meter, with the following peak wavelength (nm): 1 = 365, 2 = 385, 3 = 395, 4 = 405, 5 = 416, 6 = 450, 7 = 475, 8 = 506, 9 = 520, 10 = 590, 11 = 595, 12 = 620, 13 = 633, 14 = 655, 15 = 690, 16 = 733, 17 = 760, 18 = 770, 19 = 810. Additionally, two types of ‘white’ LEDs 20 and 21.

a

Seoul 3	Seoul 3	Seoul 3	Seoul 3	Seoul 3	Seoul 3	Seoul 3	Seoul 3	Seoul 1
Seoul 4	385 nm 1	780 nm 2	420 nm 1	760 nm 2	690 nm 2	730 nm 3	385 nm 2	Seoul 1
Seoul 4	730 nm 1	810 nm 1	475 nm 2	520 nm	850 nm 2	505 nm 2	780 nm 4	Seoul 1
Seoul 4	525 nm 1	395 nm 1	582 nm	595 nm 1	810 nm 3	385 nm 2	620 nm 2	Seoul 1
Liminus	760 nm 1	395 nm 1	630 nm	Luminus	690 nm 3	405 nm 2	595 nm 2	Luminus
Seoul 4	475 nm 1	620 nm 1	810 nm 2	940 nm	653 nm	760 nm 4	475 nm 3	Seoul 1
Seoul 4	780 nm 1	525 nm 1	505 nm 1	450 nm	850 nm 1	780 nm 3	525 nm 2	Seoul 1
Seoul 4	730 nm 2	405 nm 1	690 nm 1	760 nm 3	420 nm 2	730 nm 4	365 nm 2	Seoul 1
Seoul 2	Seoul 2	Seoul 2	Seoul 2	Seoul 2	Seoul 2	Seoul 2	Seoul 2	Seoul 1

b

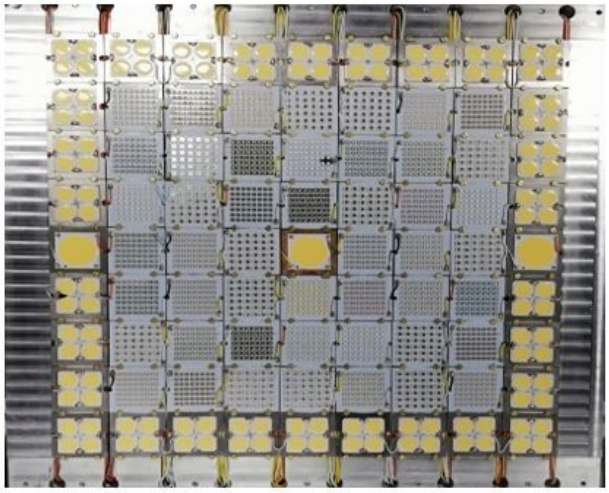

Figure 2

(a) Scheme of the inner LED lighting field with 81 aluminium core PCBs (Printed Circuit Boards) where the different LEDs are mounted on aluminium cooling body. (b) Picture of the inner LED light field prototype.

a

Seoul 3	Seoul 3	Seoul 3	Seoul 3	Seoul 3	Seoul 3	Seoul 3	Seoul 3	Seoul 1
Seoul 4	385 nm 1	780 nm 2	420 nm 1	760 nm 2	690 nm 2	730 nm 3	385 nm 2	Seoul 1
Seoul 4	730 nm 1	810 nm 1	475 nm 2	520 nm	850 nm 2	505 nm 2	780 nm 4	Seoul 1
Seoul 4	525 nm 1	395 nm 1	582 nm	595 nm 1	810 nm 3	385 nm 2	620 nm 2	Seoul 1
Liminus	760 nm 1	395 nm 1	630 nm	Luminus	690 nm 3	405 nm 2	595 nm 2	Luminus
Seoul 4	475 nm 1	620 nm 1	810 nm 2	940 nm	653 nm	760 nm 4	475 nm 3	Seoul 1
Seoul 4	780 nm 1	525 nm 1	505 nm 1	450 nm	850 nm 1	780 nm 3	525 nm 2	Seoul 1
Seoul 4	730 nm 2	405 nm 1	690 nm 1	760 nm 3	420 nm 2	730 nm 4	365 nm 2	Seoul 1
Seoul 2	Seoul 2	Seoul 2	Seoul 2	Seoul 2	Seoul 2	Seoul 2	Seoul 2	Seoul 1

b

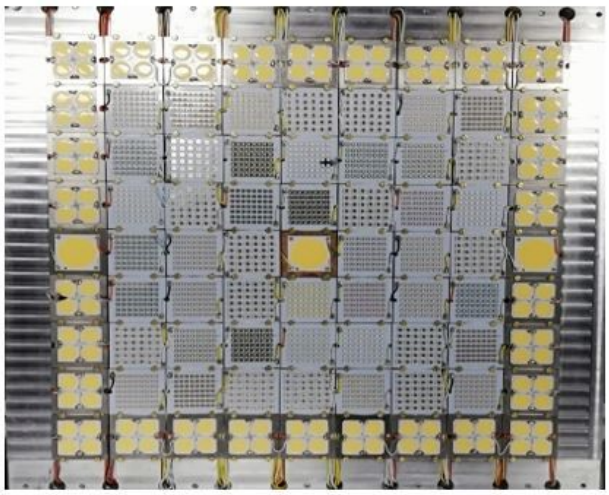

Figure 2

(a) Scheme of the inner LED lighting field with 81 aluminium core PCBs (Printed Circuit Boards) where the different LEDs are mounted on aluminium cooling body. (b) Picture of the inner LED light field prototype.

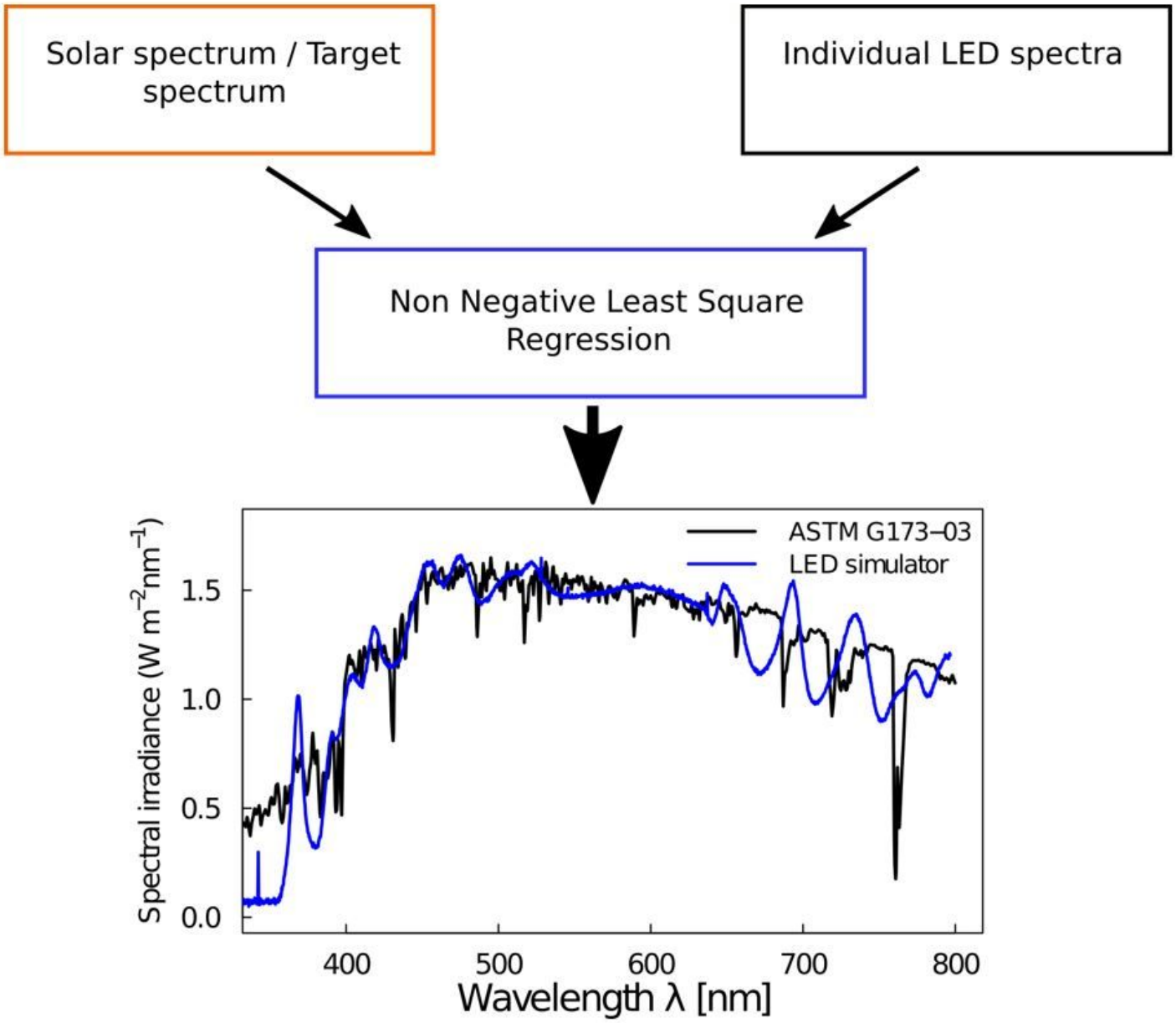

Figure 3

Workflow to generate a certain spectral irradiance. (a) Target spectrum which should be simulated. Could be the natural solar irradiance to a certain daytime, season and habitat, or an artificial spectrum. (b) Individual LED spectra shown in Figure 1 or the theoretical calculated spectra with the parameters of the corresponding manufactures' data sheets. (c) Multi linear non-negative regression based on the non-negative least square NNLS method of Lawson-Hanson algorithm. (d) Result of the workflow, target spectrum is the ASTM G173-03 spectrum and the synthesized LED spectrum.

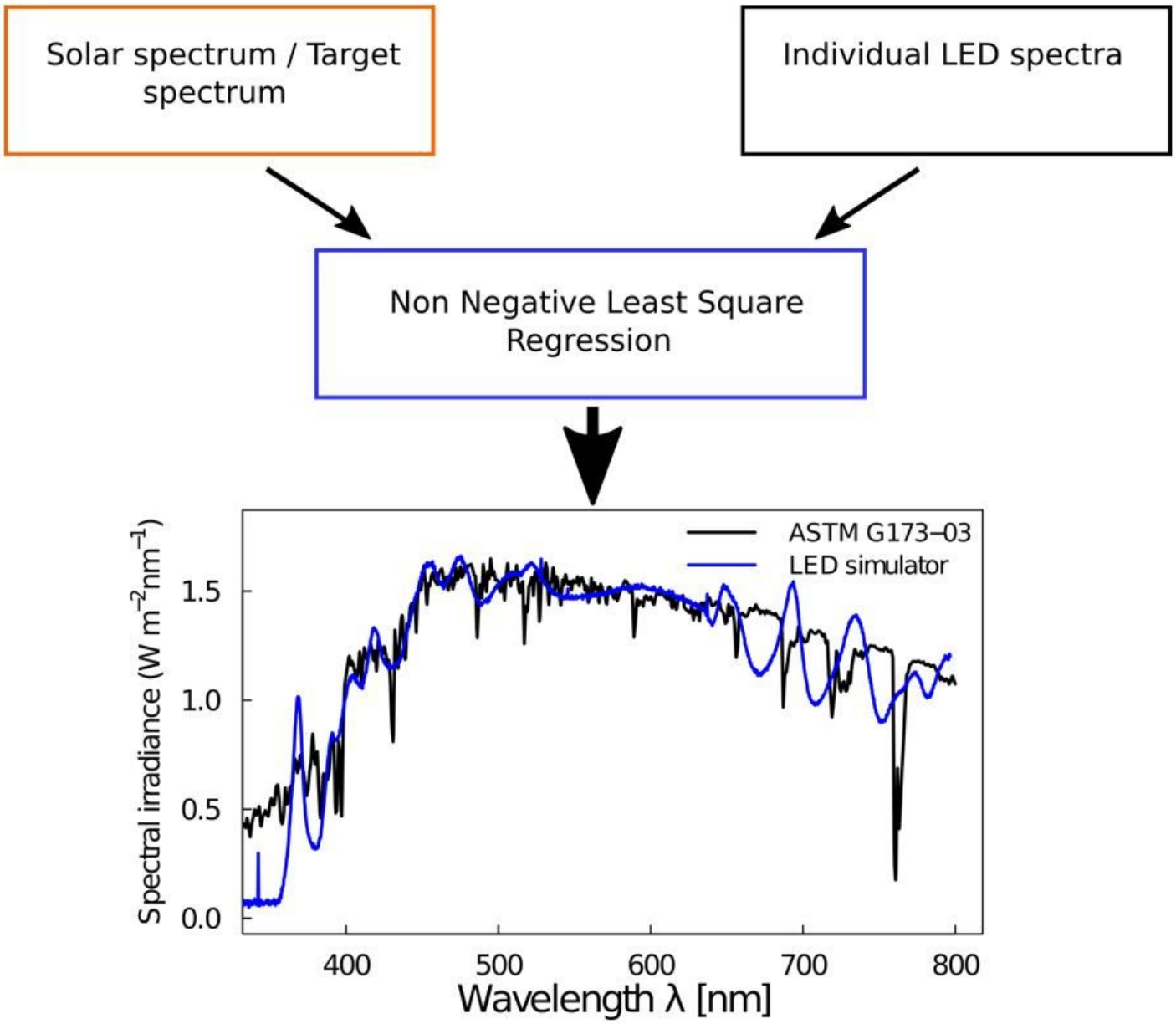

Figure 3

Workflow to generate a certain spectral irradiance. (a) Target spectrum which should be simulated. Could be the natural solar irradiance to a certain daytime, season and habitat, or an artificial spectrum. (b) Individual LED spectra shown in Figure 1 or the theoretical calculated spectra with the parameters of the corresponding manufactures' data sheets. (c) Multi linear non-negative regression based on the non-negative least square NNLS method of Lawson-Hanson algorithm. (d) Result of the workflow, target spectrum is the ASTM G173-03 spectrum and the synthesized LED spectrum.

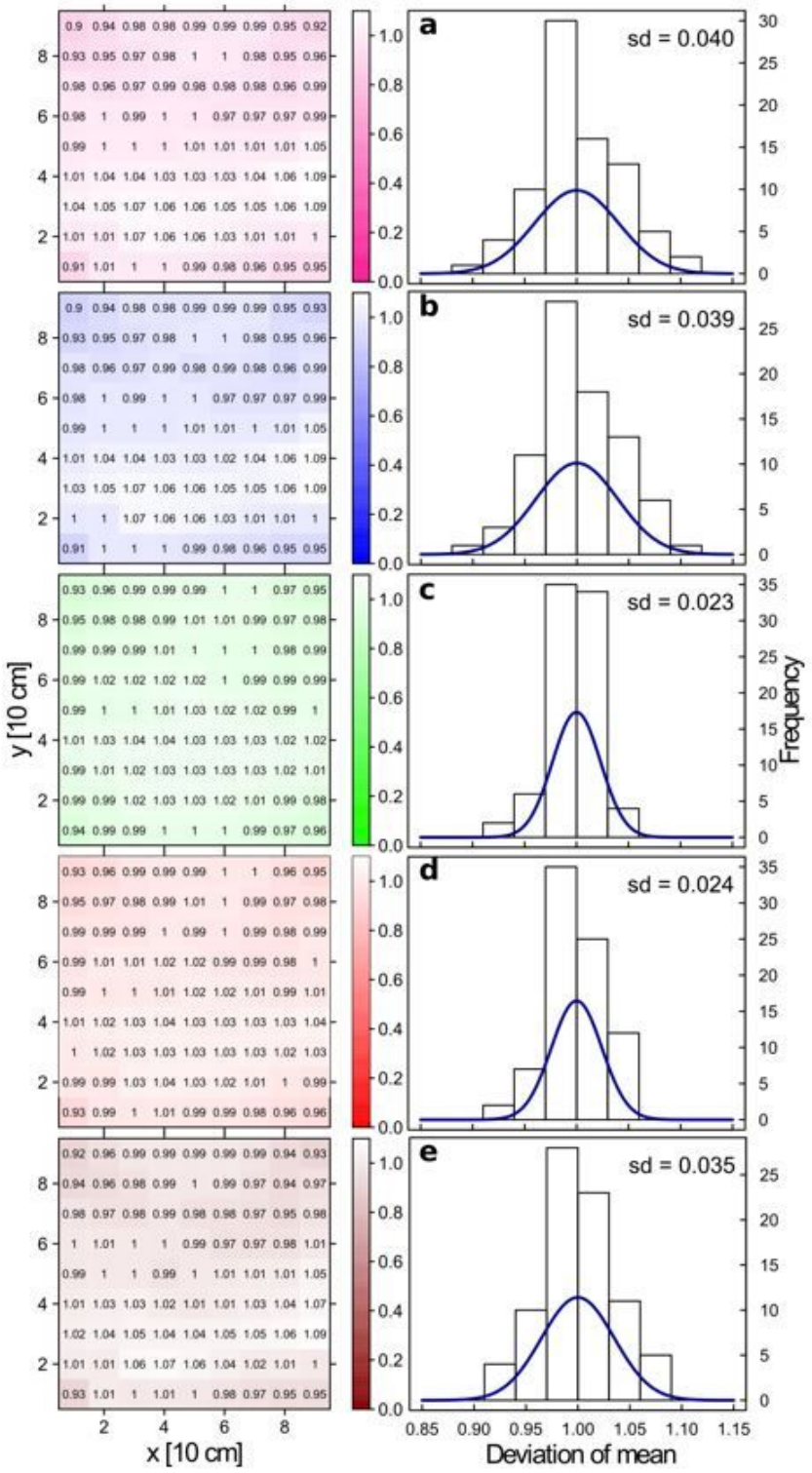

Figure 4

Spectral irradiance at different positions in the experimental space for different wavelength intervals. Every 10 cm in x direction and 10 cm in y direction the spectral irradiance was measured, resulting in a matrix with 81 positions. These 81 values were additionally plotted in a histogram. Wavelength intervals (nm.): 360-400 (a), 400-500 (b), 500-600 (c), 600-700 (d), and 700-800 (e).

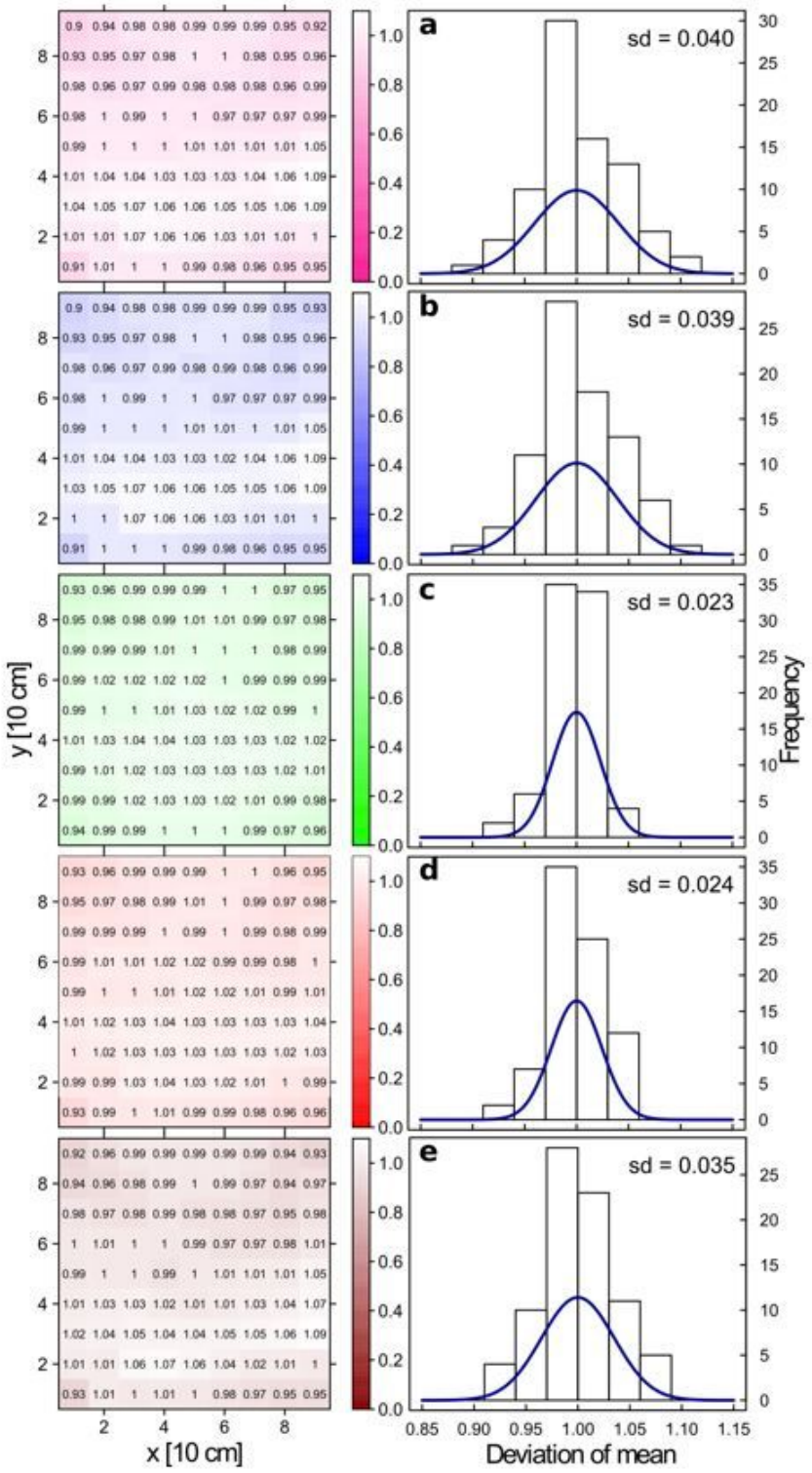

Figure 4

Spectral irradiance at different positions in the experimental space for different wavelength intervals. Every 10 cm in x direction and 10 cm in y direction the spectral irradiance was measured, resulting in a matrix with 81 positions. These 81 values were additionally plotted in a histogram. Wavelength intervals (nm.): 360-400 (a), 400-500 (b), 500-600 (c), 600-700 (d), and 700-800 (e).

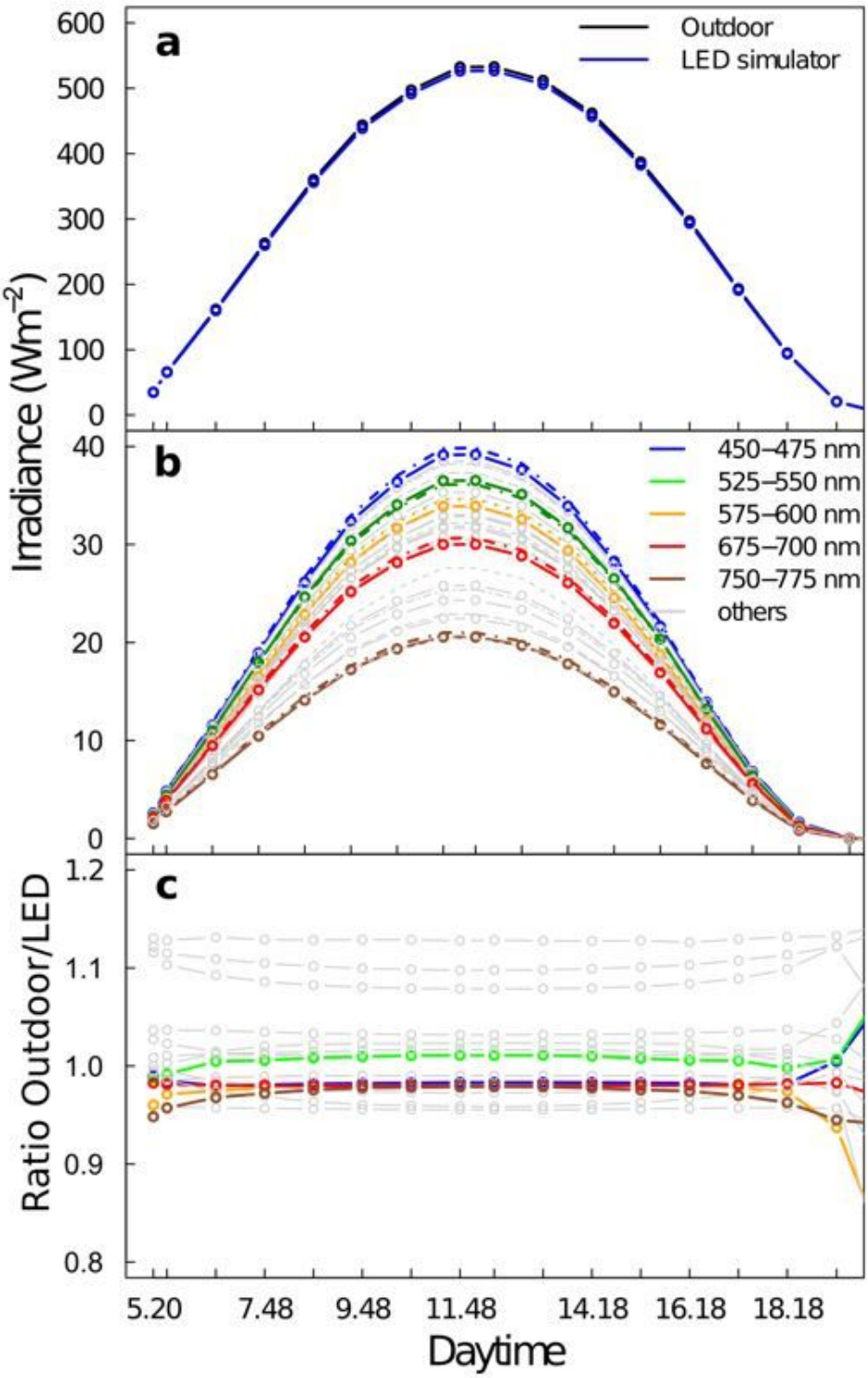

Figure 5

Diurnal variations of solar irradiance and simulated irradiance. (a) Diurnal variation of the irradiance integrated from 360-800 nm from solar irradiance spectrum compared to the composed LED spectrum. (b) Comparison for the interval 360-400 nm and then for each 25 nm an interval up to 800 nm. (c) Ratio of natural solar spectrum and synthesized LED spectra for the different wavelength intervals.

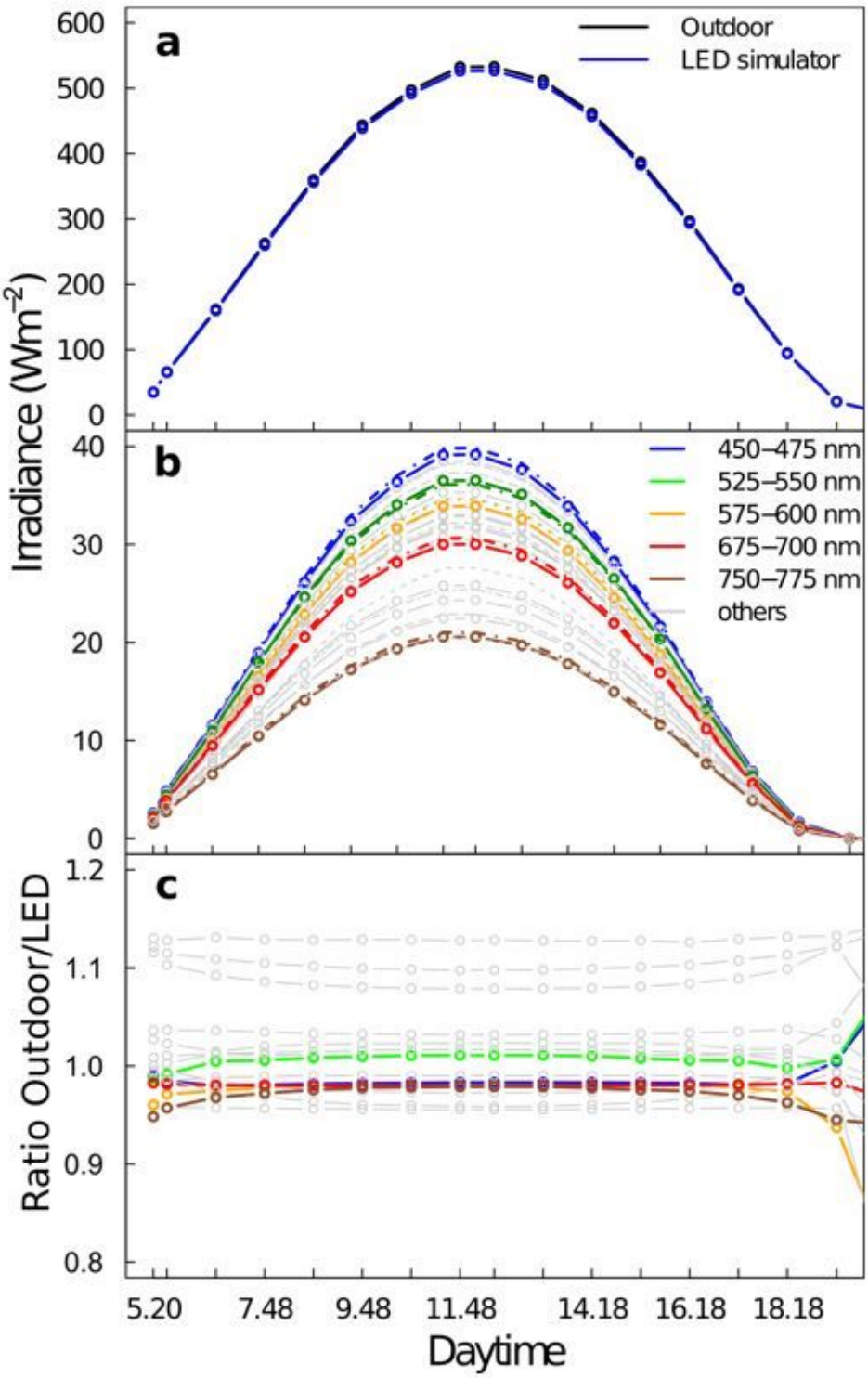

Figure 5

Diurnal variations of solar irradiance and simulated irradiance. (a) Diurnal variation of the irradiance integrated from 360-800 nm from solar irradiance spectrum compared to the composed LED spectrum. (b) Comparison for the interval 360-400 nm and then for each 25 nm an interval up to 800 nm. (c) Ratio of natural solar spectrum and synthesized LED spectra for the different wavelength intervals.

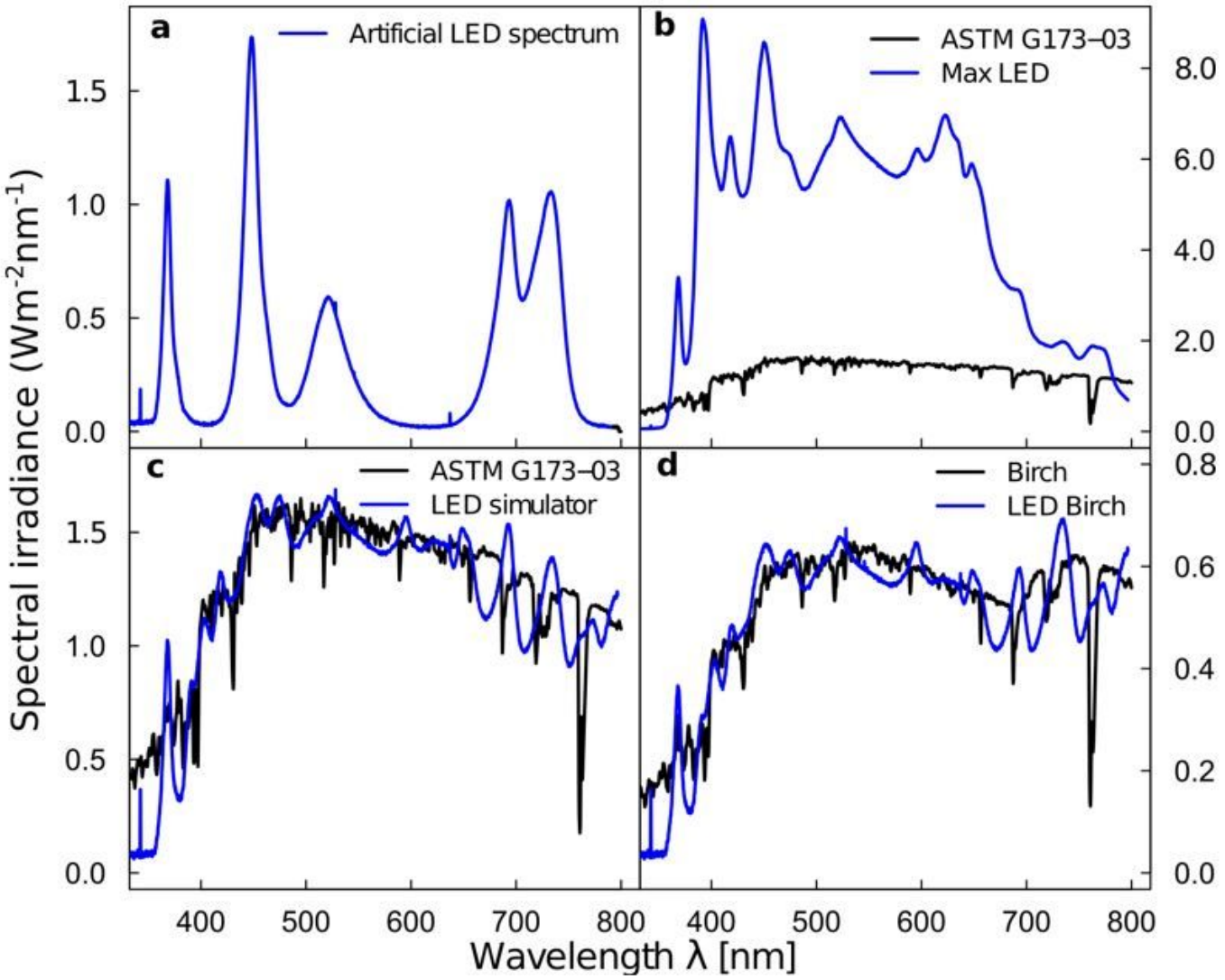

Figure 6

Different possible applications of a LED-based solar simulator. (a) Artificial spectrum for indoor/vertical farming or greenhouses. (b) High spectral irradiance of 2554 W m-2 for material science. (c) Solar spectral irradiance on a cloudless day (19 May 2007; 48°13'13.1"N 11°35'51.4"E) at 12:18 CET for human wellbeing, plant research, photovoltaics and exobiology in space. (d) Spectral irradiance under a birch tree for photobiology [49].

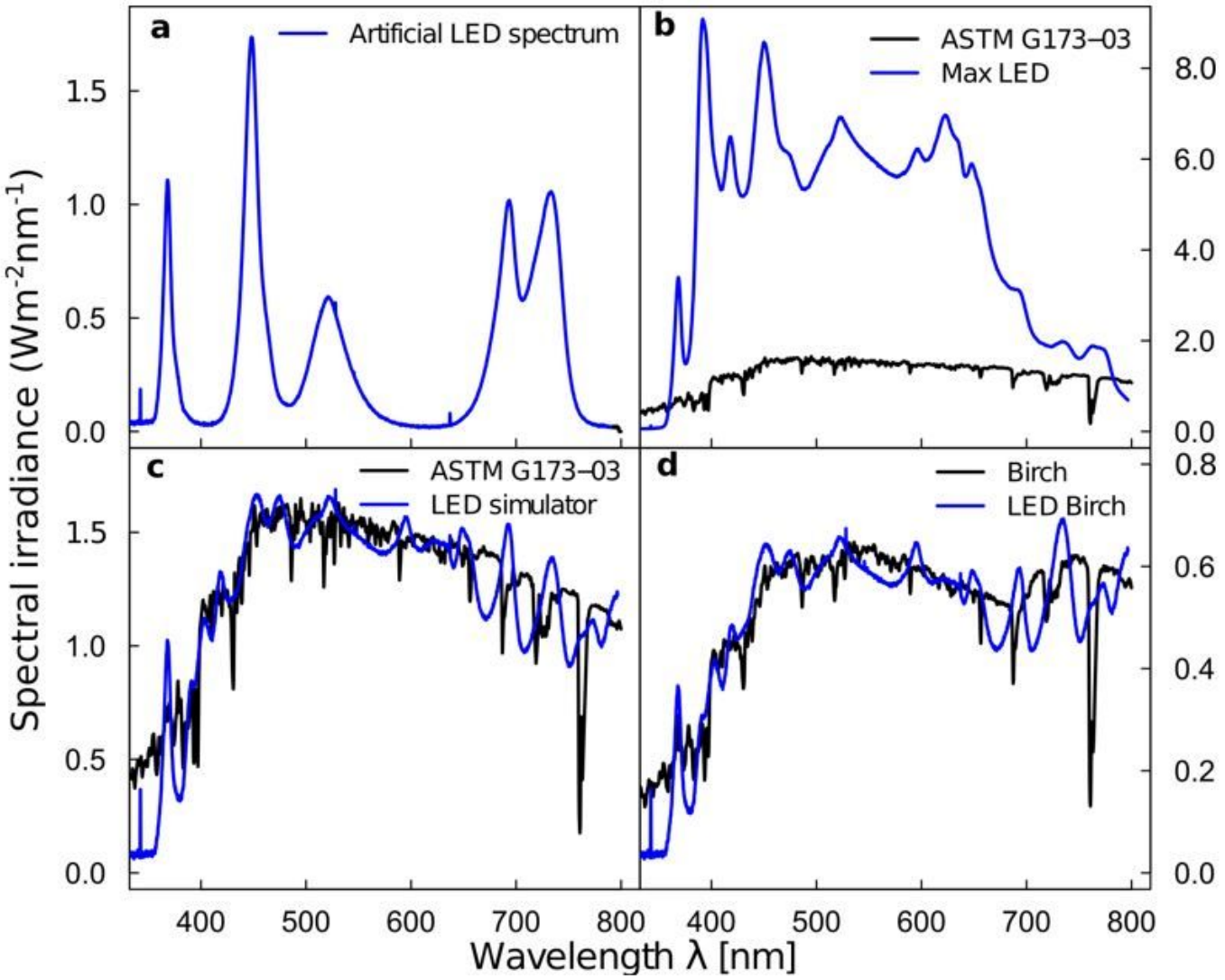

Figure 6

Different possible applications of a LED-based solar simulator. (a) Artificial spectrum for indoor/vertical farming or greenhouses. (b) High spectral irradiance of 2554 W m-2 for material science. (c) Solar spectral irradiance on a cloudless day (19 May 2007; 48°13'13.1"N 11°35'51.4"E) at 12:18 CET for human wellbeing, plant research, photovoltaics and exobiology in space. (d) Spectral irradiance under a birch tree for photobiology [49].

Supplementary Files

This is a list of supplementary files associated with this preprint. Click to download.

- Kopatschetalsupplementalfiles.pdf
- Kopatschetalsupplementalfiles.pdf